Western Washington University
Western CEDAR

Geology Faculty Publications

Geology

12-8-2011

Rock Magnetism of Hematitic "Bombs" From the Araguainha Impact Structure, Brazil

Luigi Jovane

Elder Yokoyama

Takele Seda
Western Washington University, takele.seda@wwu.edu

Russ F. Burmester
Western Washington University, russ.burmester@wwu.edu

Ricardo I.F. Trindade

See next page for additional authors

Follow this and additional works at: https://cedar.wwu.edu/geology_facpubs

Part of the Geology Commons

Authors

Luigi Jovane, Elder Yokoyama, Takele Seda, Russ F. Burmester, Ricardo I.F. Trindade, and Bernard A. Housen

Rock magnetism of hematitic "bombs" from the Araguainha impact structure, Brazil

Luigi Jovane

Department of Geology, Western Washington University, Bellingham, Washington 99225-9080, USA

Advanced Materials Science and Engineering Center, Western Washington University, Bellingham, Washington 99225-9065, USA

Now at Instituto Oceanográfico, Univerisdade de São Paulo, 191 Praça do Oceanográfico, Butantã, São Paulo 05508-120, Brazil (jovane@usp.br)

Elder Yokoyama

Departamento de Geofísica, Instituto de Astronomia, Geofísica e Ciências Atmosféricas, Universidade de São Paulo, 1226 Rua do Matão, Butantã, São Paulo 05508-090, Brazil

Takele Seda

Department of Physics and Astronomy, Western Washington University, Bellingham, Washington 99225-9080, USA

Advanced Materials Science and Engineering Center, Western Washington University, Bellingham, Washington 99225-9065, USA

Russell F. Burmester

Department of Geology, Western Washington University, Bellingham, Washington 99225-9080, USA

Ricardo I. F. Trindade

Departamento de Geofísica, Instituto de Astronomia, Geofísica e Ciências Atmosféricas, Universidade de São Paulo, 1226 Rua do Matão, Butantã, São Paulo 05508-090, Brazil

Bernard A. Housen

Department of Geology, Western Washington University, Bellingham, Washington 99225-9080, USA

Advanced Materials Science and Engineering Center, Western Washington University, Bellingham, Washington 99225-9065, USA

[1] Hematite impact "bombs" are one of the most striking (and enigmatic) features of the large Araguainha impact structure in central Brazil. They have both porous or massive textures, elongated shapes from 5 to 50 cm in diameter, and botryoidal textures that suggest hydrothermal origin. Some authors have considered these objects as a possible analog of hematite nodules found in Mars, and consequently related to a hydrothermal system. Here we report rock magnetic measurements, X-ray diffraction and Mössbauer spectra for both massive and porous samples for a detailed description of the hematite. Room temperature magnetic measurements, including hysteresis loops, back-field and saturation magnetization acquisition, FORC, as well as X-ray diffraction and Mössbauer experiments are compatible with both massive and porous types being almost pure hematite. Room temperature FORCs after heating in a He atmosphere show two peaks; the original high-coercivity peak of hematite and a low-coercivity one (probably maghemite) at the Bc and

Bb origin, thus indicating significant modification of the magnetic mineralogy of the material during thermal treatment in reducing conditions. However, conditioning in an oxidizing environment (heating in air) seemed to block generation of this low coercivity material in subsequent heating in a reducing (Ar) atmosphere. Therefore, we conclude that this material was not heated greatly in its generation. This would not be likely for impact-ejected bombs, so origin from post-impact hydrothermal activity seems likely.

1. Introduction

[2] Impact cratering is of primary importance in the evolution of solid bodies of the Solar System [e.g., *French*, 1998]. On the Earth, several studies show that the impact cratering process produced significant changes to the surface, climate and biosphere [e.g., *Shoemaker*, 1977; *French*, 2004; *Koeberl*, 2006]. During impact cratering a considerable amount of rocks is vaporized, melted and ejected, producing a great variety of new materials [e.g., *Melosh*, 1989; *French*, 1998]. One of these interesting materials can be found within a polymict breccia in the Araguainha impact structure (Brazil). In the center of this complex impact structure is a peculiar nodular hematitic material, which has been recognized as impact "bombs" by *Hippertt and Lana* [1998].

[3] The Araguainha impact structure (16°17′ S; 52°29′ W) with a diameter of ~40 km is situated between the states of Mato Grosso and Goiás, in central Brazil (Figure 1a). The impact occurred close to the Permo-Triassic boundary in the reddish siliciclastic Paleozoic formations of the Paraná Basin [e.g., *Hammerschmidt and von Engelhardt*, 1995; *Lana et al.*, 2007]. Although erosion has removed much of the impact-related materials, many impact melt rocks and polymict breccia deposits are still preserved inside the central peak [e.g., *Lana et al.*, 2008; *von Engelhardt et al.*, 1992]. Previous authors interpreted this breccia as deposits of fall back [e.g., *von Engelhardt et al.*, 1992; *Hippertt and Lana*, 1998], which formed when the some part of the ejecta blanket (deposited during the contact and excavation stages), was driven toward to the center of structure when the transient crater collapsed [e.g., *French*, 1998]. At Araguainha, polymict breccia occurs generally along the contact between the porphyritic-granite core of the impact structure and the collar of supracrustal rocks (Figure 1a). Most clasts are angular sedimentary rock (conglomerate, sandstone, siltstone and carbonate), with sizes ranging from centimeters to meters. Less abundant are clasts of porphyritic granite, metamorphic basement, and iron oxide nodules. The iron oxide nodules are composed almost exclusively of hematite. Vesicular-like and feather-like structures in them suggest origin from melting and ejection of hematite sandstones target rocks [*Hippertt and Lana*, 1998]. Those hematite "bomb-like" nodules range from 5 to 50 cm in diameter with various geometries and both "Porous" and "Massive" texture (Figure S1 in the auxiliary material).[1] Porous hematite "bombs" have irregular shapes and no "aerodynamic" features. They are of centimeter-size with elongated shape and filled with the same material. By contrast Massive hematite "bombs" are characterized by concave and convex surfaces, which have been interpreted by *Hippertt and Lana* [1998] as aerodynamic structures expressed as conical wedge-shaped units and

———————————————
[1]Auxiliary materials are available in the HTML. doi:10.1029/2011GC003758.
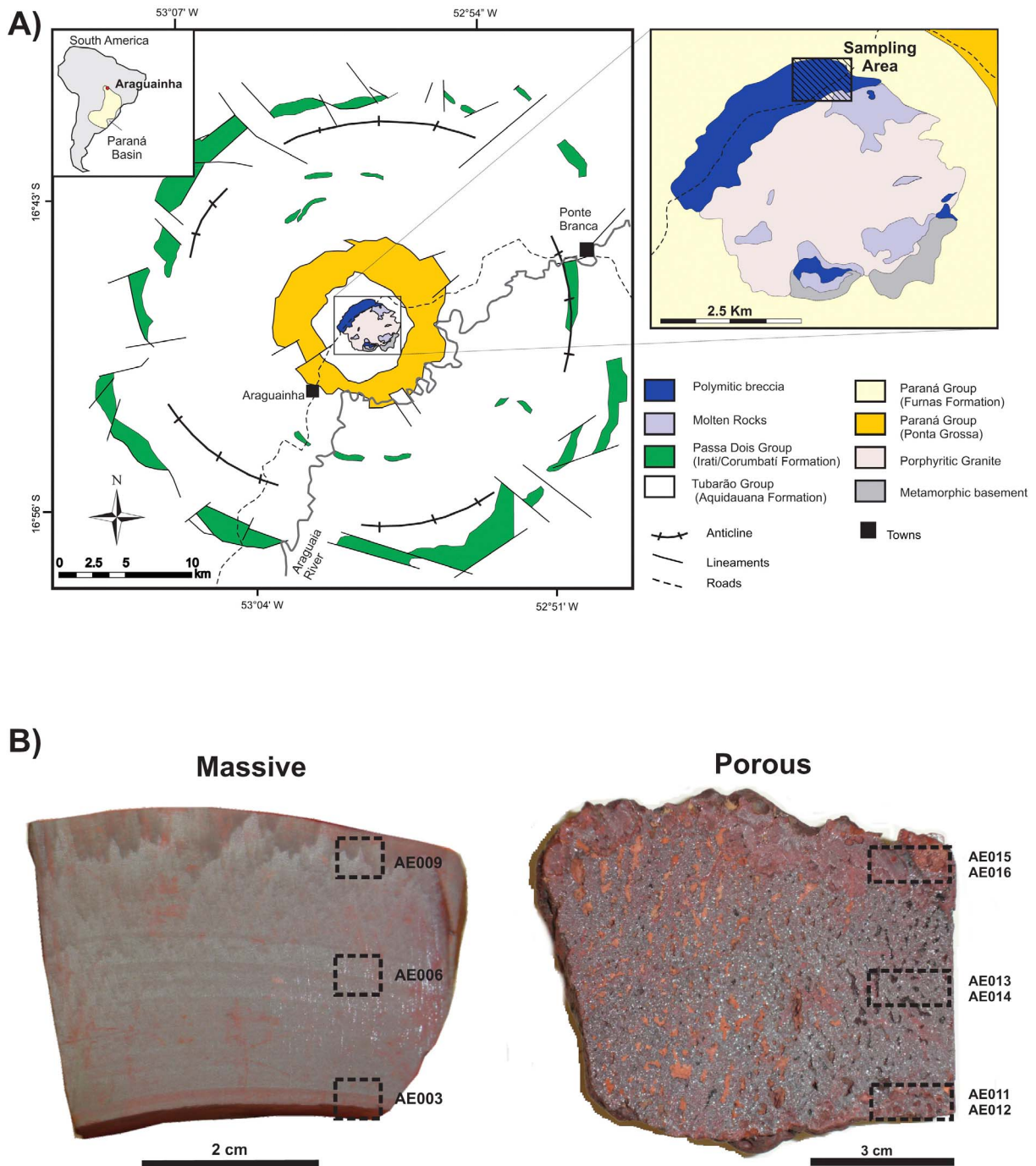
Figure 1. (a) Simplified geological map of the Araguainha impact structure with the location of the sampling area; (b) Porous and Massive samples found in the center of the crater. Rectangular areas show where the samples were taken, but the size is not related to the specimen dimensions.

asymmetrical ripples due to atmospheric ablation. However, those same features, at the external surface of the Massive type and some internal surfaces of the Porous type (Figure S2), can be interpreted as botryoidal textures similar to those found in hematite-rich deposits of hydrothermal origin found elsewhere [*Wernicke and Lippolt*, 1993, 1997].

[4] Although the two types, Massive and Porous, are similar in composition, they may have originated under different conditions. Distinguishing between them may be important to understanding the evolution of the Araguainha impact structure, and possibly similar hematite concentrations elsewhere on Earth and on Mars. For example, data

from Mars Global Surveyor suggest an important link between strong impact events on that planet and the setting of major magnetic anomalies on Mars's crust [e.g., *Acuña et al.*, 1999; *Arkani-Hamed*, 2002; *Mohit and Arkani-Hamed*, 2004]. Nevertheless, the origin of these anomalies, especially the mineral carriers of remanent magnetization on Mars's crust, remains a matter of debate in literature [e.g., *Kletetschka et al.*, 2000a; *Rochette et al.*, 2001, 2003; *Dunlop and Arkani-Hamed*, 2005; *Carporzen et al.*, 2005]. Pyrrhotite, hematite and magnetite are the strongest candidates to carry Mars's magnetization. For example, hematite deposits on Mars have been identified by the rover Opportunity (imaged hematite spherules embedded in rock at the landing site) and the sondes Mars Global Surveyor and Mars Odyssey [cf. *Arvidson et al.*, 2006]. Production of these deposits on Mars surface has been attributed to a hydrothermal system associated with volcanic activity [*Arvidson et al.*, 2006]. However, an impact origin of the nodules is not excluded [*Catling and Moore*, 2003]. *Catling and Moore* [2003] debate that Martian hematite nodules could have been generated by melting, which is the mechanism first proposed by *Hippertt and Lana* [1998] for the hematitic material found at the Araguainha impact structure. Therefore, the study of the magnetic properties of these objects may help resolve the debate about the origin of this materials and presence of water on Mars.

[5] Since both types are almost exclusively composed of hematite, a common magnetic minerals, analysis of their magnetic properties under different conditions that might mimic redox environment of an impact plume, melting for the high pressures and rapid cooling after impact in particular atmospheric conditions, may contribute to our understanding of their genesis. Here we report rock magnetic, X-ray diffraction and Mössbauer spectroscopy measurements for these hematite materials in order to determine if the "bombs" origin is feasible.

2. Samples and Methods

[6] We collected hand-samples of the hematitic material from the main outcrop of polymict breccia in the impact structure, in the north-northeast sector of the central area, along the road from Araguainha to Ponte Branca cities (Figure 1a). These samples represent both Porous and Massive types [*Hippertt and Lana*, 1998]. For both types, nine cubic samples (8 mm³) were obtained at different depths below the external surface of the original "bombs"

(Figure 1b). Rock magnetic, X-ray diffraction and Mössbauer spectroscopy measurements were made on the same samples in order to understand the origin and composition of this material.

[7] We measured susceptibility-versus-temperature (thermomagnetic curves) using the KLY-4 (AGICO) Kappabridge susceptometer and CS-3 furnace at the Instituto de Astronomia, Geofísica e Ciências Atmosféricas, Universidade de São Paulo (IAG-USP). This instrument has an operating frequency of 875 Hz and magnetic induction of 300 μT (noise level 3 X 10^{-13} m³). The powdered samples were heated progressively up to 700°C in an argon (Ar) atmosphere. Also in argon, low-temperature magnetic susceptibility was recorded using a CS3-L apparatus coupled to the KLY-4 susceptometer from about −196°C to room temperature. Inflection points on the thermomagnetic curves were graphically estimated through the software Cureval 8 (AGICO) and by second derivatives through the software RockMag Analyzer 1.0 [*Leonhardt*, 2006].

[8] We measured hysteresis loops, saturation magnetization (Ms), saturation remanent magnetization (Mrs), and coercive force (Bc) using the Princeton Measurements MicroMag model 3900 vibrating sample magnetometer (VSM) of the Pacific Northwest Paleomagnetic Laboratory at the Geology Department, Western Washington University (WWU). Using the same instrument, we also measured the stepwise acquisition of Mr (after alternated field (AF) demagnetization), and back-field demagnetization to determine the remanent coercivity (Bcr), in addition to first-order reversal curve (FORC) experiments. The VSM furnace allowed these measurements to be made at temperatures up to 700°C in helium atmosphere. Runs at temperature lasted about 2 h. We made similar measurements at room temperature after most temperature steps, and on separate sister samples after each heating step with different heating protocol. The sister samples were processed in an ASC thermal demagnetizer at WWU and held at temperature for minimum of 3 h. They were first heated and cooled in air (~20% O₂) in steps up to 700°C, then reheated to 700°C for four hours in argon atmosphere. This was to document the effects of oxidation during heating and test for reduction afterwards.

[9] A FORC distribution is built from a series of partial hysteresis curves. After inducing a strong positive field, the sample's magnetic moment is measured while decreasing the inducing magnetic field to a negative and smaller value (Ba). Then, the

magnetic moment is measured while the field (Bb) is gradually increased from Ba to the saturating field. This process is repeated for several values of Ba building a family of curves. The second derivative of the curves with respect to Ba and Bb allows building a contour plot, which is the FORC distribution [*Pike et al.*, 1999; *Roberts et al.*, 2000; *Muxworthy and Roberts*, 2006]. A FORC distribution allows defining qualitative analysis on microcoercivity distributions and magnetic interactions between magnetic grains in the sample. FORC diagrams here were created using FORCIT software [*Acton et al.*, 2007] and FORCinel [*Harrison and Feinberg*, 2008]. In order to study the samples' thermal stability under heating we performed a series of FORC measurements at increasing temperatures of 100, 200, 350, 450, 550, 600, 650 and 700°C in helium. Hysteresis loops, magnetization acquisition and back-field demagnetization of saturation remanence, and FORCs have been measured after heating in argon and open air atmosphere to study the oxidation of the magnetic minerals. The same parameters have been measured in open air atmosphere after heating for 5 h at 100, 200, 350, 450, 550, 600, 650 and 700°C.

[10] Mössbauer spectra and XRD patterns were acquired at WWU. Mössbauer spectra were recorded at room temperature with a constant-acceleration spectrometer (Wissel GMBH, Germany) in a horizontal transmission mode using a 50 mCi ^{57}Co source. The velocity scale was normalized with respect to metallic iron at room temperature. The Mössbauer spectra were fitted by assuming Lorentzian line shapes using the NORMOS (Wissel GMBH) least squares fitting program. In fitting the spectra, magnetic hyperfine splitting with six lines corresponding to the single Fe^{3+} site was used for each spectrum.

[11] X-ray diffraction (XRD) patterns of the samples were obtained using a PANalytical X'Pert Pro diffractometer equipped with a monochromatic Cu-K$_\alpha$ source (λ = 1.54050 Å). An appropriate amount of sample was mixed with a small amount of acetone and the mixture deposited onto a microscope slide. Following evaporation of the acetone, the microscope slide was mounted on the sample stage for XRD pattern acquisition.

3. Results

3.1. Measurements at Room Temperature

[12] Hysteresis loops, back-field and saturation magnetization acquisition after AF demagnetization,

at room temperature show that complete saturation was not achieved for all samples at 1T, the maximum inducing field used for most samples in this study (Figures 2a and 2b). Although we have corrected the hysteresis curves for a constant high field paramagnetic slope, we therefore assume that, for those samples, the Ms values derived from our measurements are in fact underestimated. Yet, given the almost horizontal nature of the curve at high fields for almost all samples, we suggest that this value is indeed close to saturation. The hysteresis parameters (Table 1) for all samples were represented in a Day plot, with Mrs/Ms against Bcr/Bc (Figure 2d), to obtain information about magnetic domain state and magnetic grain size. Results show that similar magnetic carriers are present in Massive and Porous types [*Day et al.*, 1977; *Dunlop*, 2002]. Nonetheless, the saturation behavior of most samples of Porous material is characterized by a sharp drop on reversing the field. After a peak in induced magnetization (our "saturation"), the magnetization slightly decreases for positive fields and abruptly decreases when the field is applied in the opposite direction (Figures 2b and 2c). Remanent magnetization acquisition and back-field curves (Figure 2c) show the same behavior. We did not succeed in completely saturating these samples, even for inducing fields as high as ~1.8 T. We also tested for anisotropy of the samples to insure that their orientation in the VSM had no effect on the result. Hematite itself is highly anisotropic, and if the material were made of aligned hematite crystals, the properties measured in different orientations would vary. Our test measured the induced magnetic moment while the sample was rotated 360° relative to the applied field. We observed no variation in moment so judge that results of other experiments are independent of sample orientation.

[13] FORC diagrams at room temperature illustrate the presence of an elongated peak between 400 and 700 mT, but with different distributions among the samples. Sample AE016 from the external part of the Porous sample shows (Figure 2e) a wide peak that starts at ~200 mT but does not end before 800 mT, showing that the magnetization does not reach saturation. However, the highest values on the contour are attained at 600–700 mT on the Bc axis, suggesting this is the most common coercivity. The peak delineates an asymmetric linear crest with highest values of Bb between 20 and −180 mT (Figure 2e). Below the crest there is a negative area. No peak is visible at the Bb and Bc origin. The FORC of sample AE012 (Figure 2f),
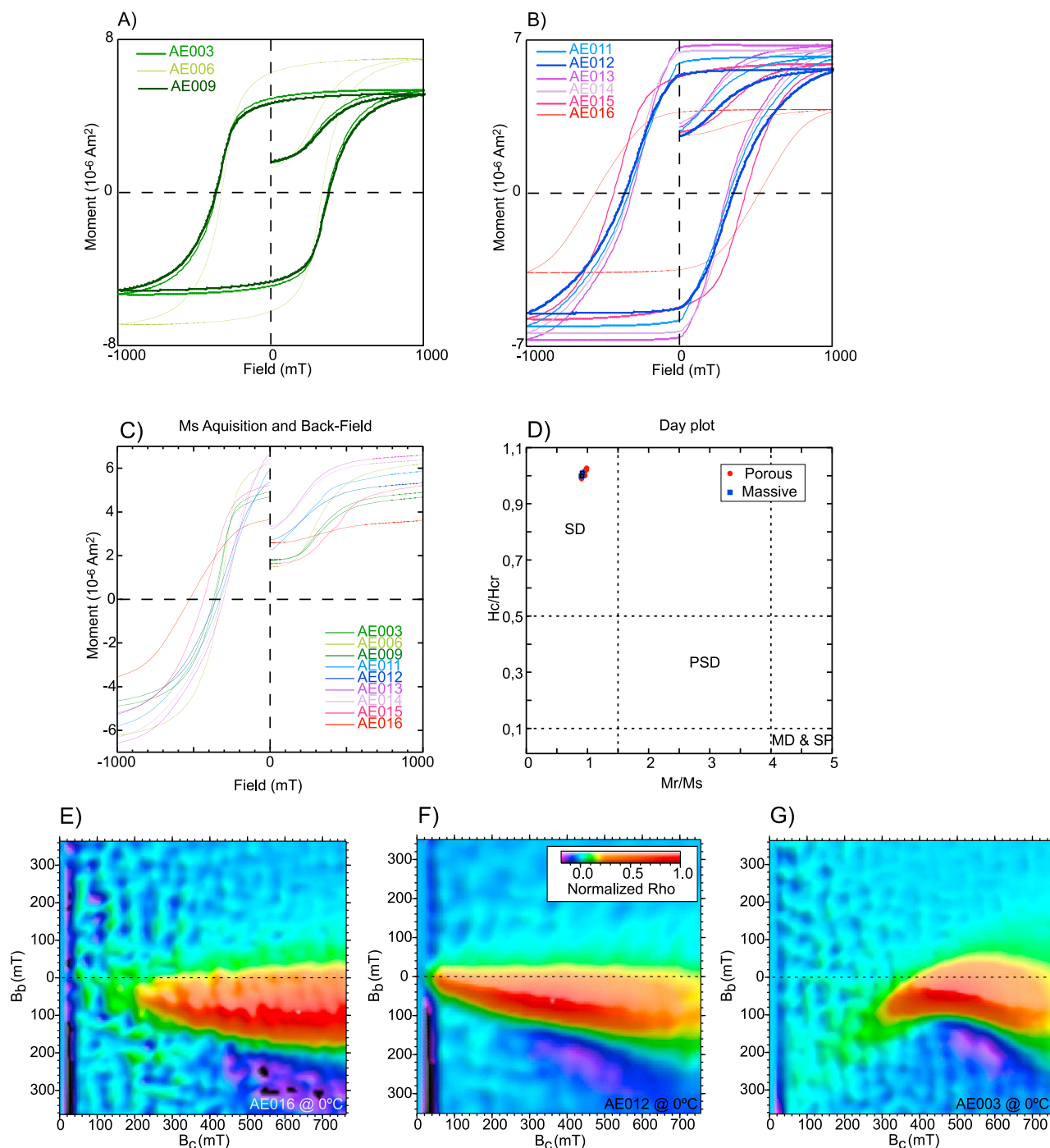
Figure 2. (a and b) Hysteresis loops; (c) back-field and Ms acquisition for all samples; (d) Day plot [*Day et al.*, 1977; *Dunlop*, 2002] representation of the hysteresis parameters; (e–g) FORC (first order reversal curve) at room temperature for Porous (Figure 2e: AE016 and Figure 2f: AE012) and Massive (Figure 2g: AE003) types. The Gaussian filtering at 126 mT is necessary to remove noise inherent in the data, which is amplified when the derivatives are taken. Scale is constant for all diagrams, which were produced with FORCIT. Massive samples show "banana" shape features (see text) and Porous samples shows a strongly shifted peak and a negative area below it. Some porous samples could not be saturated.

from the internal part of the Porous sample, has a wide peak starting from ~60 mT that delineates an asymmetric crest beneath the Bc axis (from ~40 to ~−120 mT), and decreases at Bb values of 300–

400 mT. The FORC distribution of sample AE003 (Figure 2g), which is from the external part of the Massive sample, has an asymmetric arched structure with a peak at Bc ~500 mT and Bb ~−50mT.

Table 1. Rock Magnetic Values for Hysteresis Parameters and Their Ratios

Sample	Weight (mg)	Mrs (10^{-6} Am$_2$)	Ms (10^{-6} Am$_2$)	Hc (mT)	Hcr (mT)	Mr/Ms	Hc/Hcr
AE003	159.10	4.897	5.342	362	359	0.917	1.009
AE006	178.30	6.227	6.925	327	327	0.899	0.999
AE009	157.40	4.663	5.120	370	370	0.911	0.999
AE011	238.00	5.871	6.155	330	329	0.954	1.005
AE012	217.30	5.315	5.560	355	354	0.956	1.001
AE013	254.70	6.620	6.724	311	305	0.985	1.021
AE014	246.30	6.375	6.460	327	318	0.987	1.027
AE015	191.80	5.262	5.818	431	435	0.904	0.990
AE016	161.00	3.598	3.772	536	527	0.954	1.017

This feature tends to create a particular geometry hereafter referred to as a "banana" shape.

[14] Room temperature magnetic measurements as well as X-ray diffraction patterns and Mössbauer spectra are consistent with hematite. Hyperfine interaction parameters (isomer shift, quadrupole and magnetic hyperfine splitting) are all indicative of hematite (Figure 3a). XRD spectra have 2-theta peaks at ~23, ~32, ~36, ~41, ~49, ~54, ~57, ~63, ~64 and ~72 degrees, which are comparable with pure hematite (Figure 3b).

3.2. Thermomagnetic Measurements

[15] Susceptibility-versus-temperature heating curves in argon atmosphere (Figures 4a and 4c) show an increase in magnetic susceptibility starting at 400°C, then a decrease around 580°C. During cooling the magnetic susceptibility increases slightly at 650°C, then greatly more just below 580°C. Both the increase above 400°C on heating and below 580°C on cooling are consistent with reduction of some of the hematite to magnetite or structural change to maghemite. The susceptibility-versus-temperature curves for low temperatures show the Morin transition of hematite over a temperature-range from about −60°C to −10°C for (Figures 4b and 4d).

[16] Measurements of samples heated in helium atmosphere included hysteresis loops, magnetization acquisition and back-field demagnetization of saturation remanence, and FORCs at temperature steps. Figure 5 shows FORC distributions for selected samples from Massive and Porous material. For the 100°C, 200°C, 350°C and 450°C temperature steps the peak in FORC distribution that occurs below the Bc axis narrows down and moves toward the origin while keeping the same shape observed in room temperature measurements (Figures 5a, 5b, and 5c). Beginning at the 550°C step the FORC distribution shows a small peak near

the Bc and Bb origin, and a major decrease of the peak below the Bc axis (Figures 5d and 5e). The FORC for the temperature step of 650°C has a smooth distribution on the Bc axis from the origin up to 300 mT, with a marked peak at 100 mT (Figure 5f). Finally, this low-coercivity peak disappears at the 700°C step for all samples (Figure 5g). Interestingly, the peculiar behavior in the hysteresis loops of Porous material samples disappear after heating showing that temperature affects the magnetic behavior irreversibly. Figures 5h, 5i, and 5j show some representative results after heating experiments in helium atmosphere. FORC diagrams for all samples after heating show two peaks: a low-coercivity peak at the Bc and Bb origin, and a high-coercvity peak, which corresponds to the "banana" shape peak for Massive samples, or the linear crest below the Bc axis for Porous samples. Porous and Massive types show the same magnetic features.

[17] The results from the sister samples, which were heated in air and measured at room temperature, demonstrate that there were only minor variations in hysteresis loops and FORCs after each heating step. The most important observation is that no peak is visible at the Bb and Bc origin after heating as there was after heating in helium (Figure S3a). Those sister samples were subsequently re-heated in argon atmosphere up to 700°C, but this also did not produce a peak at the Bb and Bc origin (Figure S3b). Thus, the formation of the peak at the Bb and Bc origin is only recognized for virgin samples heated up to 700°C in helium atmosphere.

[18] Mössbauer spectra after heating in helium atmosphere (Figures 3a and 3b, samples AE003 and AE016) shows a sextet, which was consistent with pure hematite (Table 2) [Gaviría et al., 2007]. XRD spectrum after heating has peaks that are relative to pure hematite with counting of the peaks similar that are comparable to synthetic hematite [Gaviría et al., 2007]. Massive and Porous materials
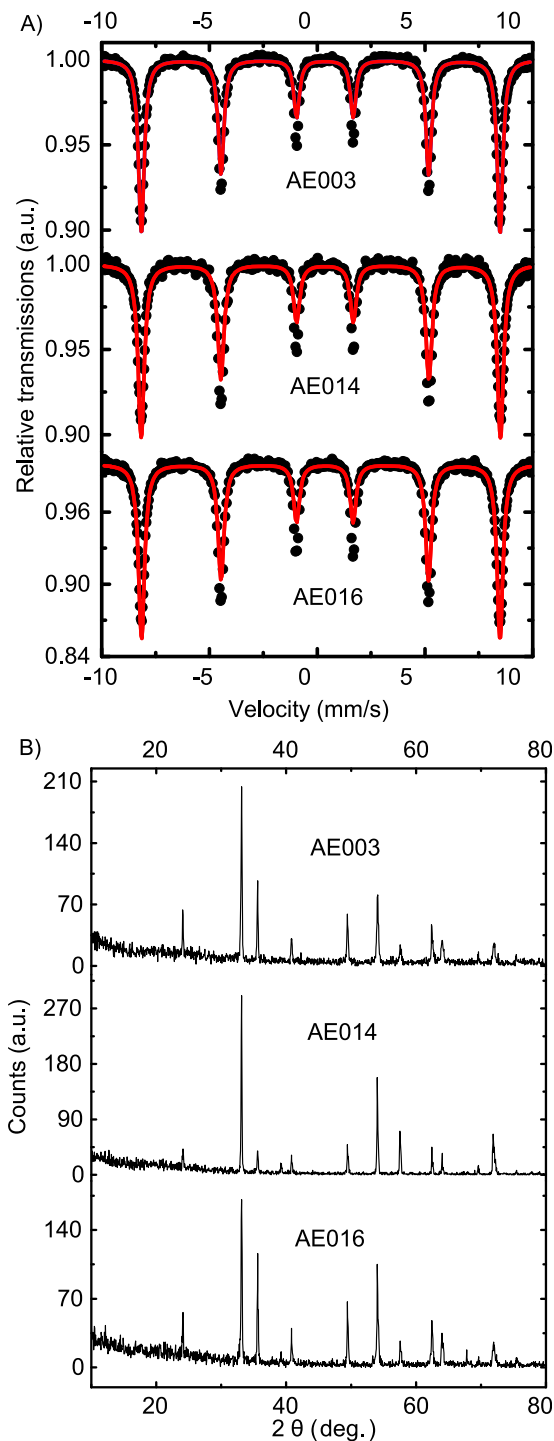
Figure 3. (a) Mössbouer and (b) XRD spectra of AE014 (not heated), AE003 and AE016 after heating at 700°C in helium atmosphere. For AE003 and AE016 reflection peaks are completely consistent with pure hematite. AE014 shows higher counts for the peaks at ~36, ~54, ~57 and ~72 degrees.

do not show compositional differences in Mössbauer and XRD spectra.

4. Discussion

4.1. Measurements at Room Temperature

[19] Presence of a very high coercivity magnetic mineral as the only magnetic mineral in virgin samples is shown from hysteresis parameters, back-field and magnetization acquisition curves at room temperature (Figure 2). The values of all magnetic parameters are compatible with hematite (α-Fe_2O_3), which is the hexagonal polymorph of ferric oxide and most stable of natural iron oxides at the earth's surface. All samples from both the Massive and Porous types show these characteristics but most of the samples of Porous material could not be saturated in the maximum inducing field of 1T used for most experiments.

[20] FORC distributions at room temperature demonstrate the presence of a high coercivity magnetic mineral. The highest values on the contour around 600–700 mT on Bc axes and an asymmetric crest of the peak in the FORC distributions for sample AE016 (from the external part of the Porous material) mean (Figure 2e) that there is a high coercivity magnetic mineral which is almost saturated at 1T. The fact that the peak distribution is situated asymmetrically, below and parallel to the ridge along the zero bias axes (Bb = 0), is due to the magnetization lying in the basal crystallographic plane of hematite [*Muxworthy et al.*, 2005; *Carvallo et al.*, 2006]. The negative area below the crest of the elongate peak from 200 mT to the end of the diagram is possibly an artifact of the fitting of the piecewise second-order mixed polynomial surface [*Muxworthy et al.*, 2005]. No peak is visible at the Bb and Bc origin meaning that any low coercivity mineral is absent before thermal treatment. The FORC of sample AE012 (Figure 2f), from the internal part of the Porous sample, has a wide peak and an asymmetric crest, but the main peak has lower values (300–400 mT) and the crest is nearer to the Bc axis compared with AE016. In contrast, the FORC distribution of sample AE003 (Figure 2g), which is from the external part of the Massive sample, has maximum values close to those of AE016. This sample is characterized with a "banana" shape peak, although it is not as elongated as the peaks of the Porous material, that lies below Bb = 0. We speculate that this peak derives at least in part from a component of the magnetization lying in the basal crystallographic plane of hematite [*Muxworthy*
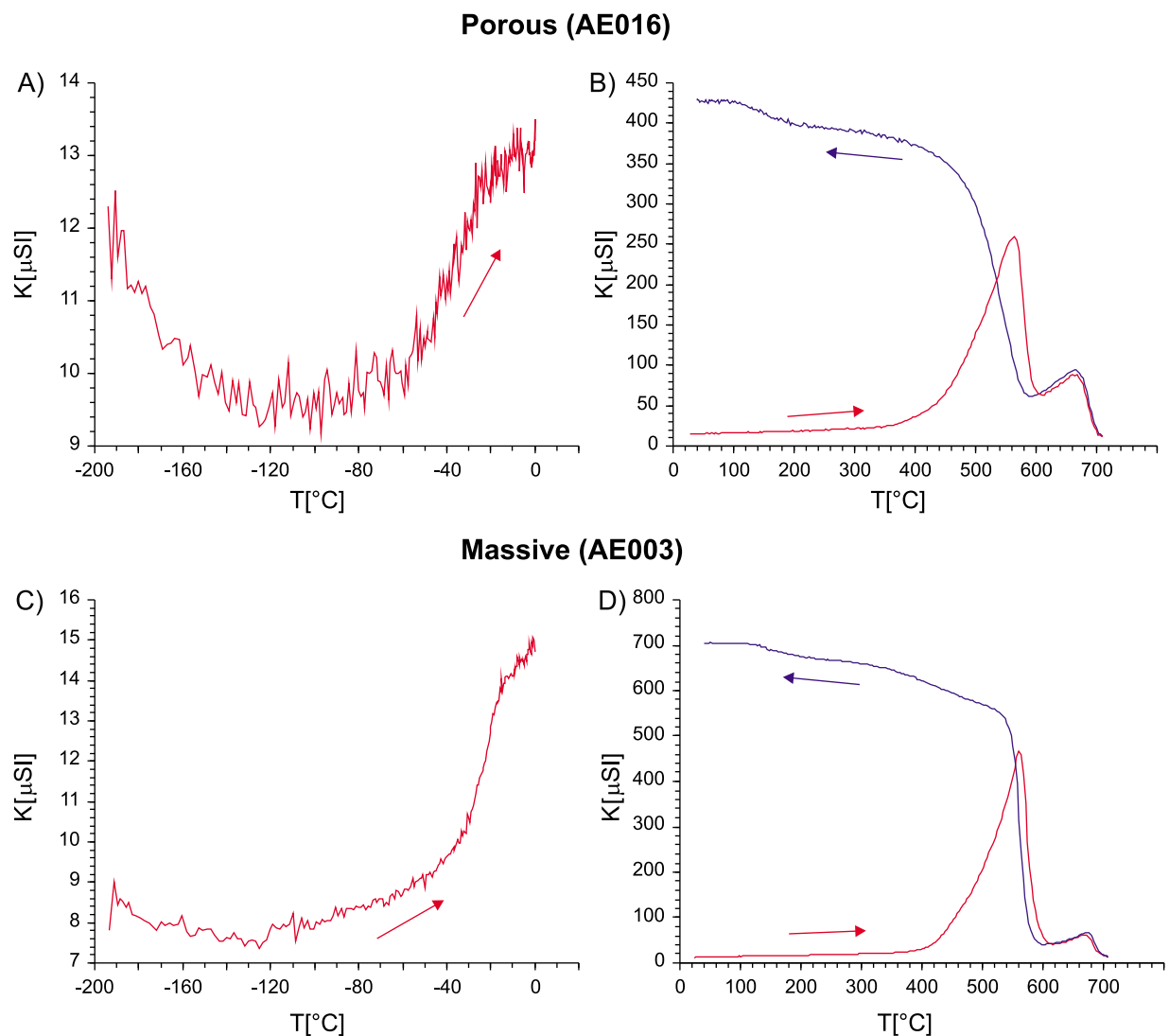
Porous (AE016)

Massive (AE003)

Figure 4. Susceptibility versus temperature curves from −196°C to 0°C and 20°C to 700°C for representative samples (AE016 and AE003).

et al., 2005; *Carvallo and Muxworthy*, 2006]. This kind of distribution has been also recognized for the iron sulphide pyrrhotite ($Fe_{1-x}S$ (x = 0 to 0.2)), which also has strong basal plane anisotropy [*Larrasoaña et al.*, 2007; *Weaver et al.*, 2002; *Roberts et al.*, 2010]. For all samples, there is no peak visible at the Bb and Bc origin, meaning that there is no occurrence of low-coercivity mineral before thermal treatment [*Carvallo et al.*, 2006].

4.2. Thermomagnetic Measurements

[21] The increase in susceptibility in thermomagnetic curves (susceptibility versus-temperature) close to 400°C suggests that a new magnetic material with high susceptibility is produced during heating (Figures 4b and 4d). This new magnetic material loses susceptibility near 580°C, thus strongly suggesting the formation of magnetite or maghemite. We suggest that the increase in susceptibility between ~400°C and ~580°C is due to the transformation of hematite into maghemite due to reduction of powdered hematite [e.g., *Petrovský et al.*, 1996]. The dramatic increase in susceptibility on cooling below 580°C shows that magnetite/maghemite generation is irreversible. Nevertheless, the presence of an initial increase in susceptibility above 650°C indicates that only a fraction of the original hematite was reduced during heating. The presence of hematite is confirmed by the low susceptibility-versus-temperature curves that show the Morin transition temperature-range from −60°C to −10°C (Figures 4a and 4c).

[22] During the 100°C, 200°C, 350°C and 450°C heating steps in helium atmosphere, the peak in the
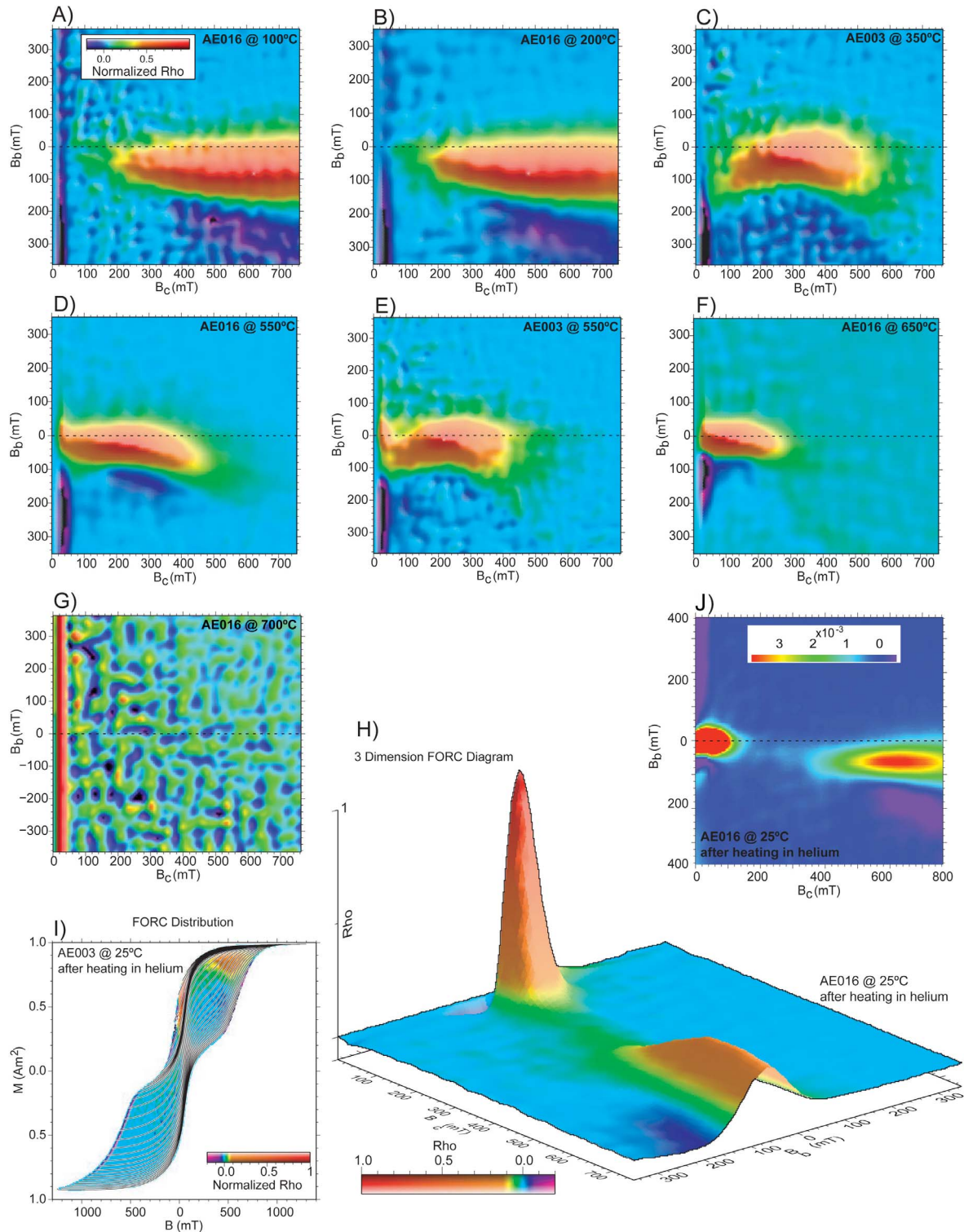
Figure 5. FORCs at various temperatures: (a) 100°C for sample AE016; (b) 200°C for sample AE016; (c) 350°C for sample AE003; (d and e) 550°C for samples AE016 and AE003, respectively; (f) 650° and (g) 700°C for sample AE016; (h) 3D FORC for sample AE016; (i) FORC distribution for sample AE003 at 25°C after annealing in argon and open air atmosphere. The Gaussian filtering at 126 mT is necessary to remove noise inherent in the data, which is amplified when the derivatives are taken. Scale is the same for Figures 5a–5g produced with FORCIT; (j) AE016 FORC distribution at 25°C annealing produced with FORCinel (smoothing factor of 3) is the 2D (horizontal) view of Figure 5h.

Table 2. Mössbouer Parameters

Sample	δ^a (mm/s)	ΔE_Q^b (mm/s)	B_{hf}^c (T)	Γ^d (mm/s)
AE014	0.375(1)	−0.192(1)	51.694(6)	0.338(2)
AE016	0.372(1)	−0.189(1)	51.578(4)	0.324(2)
AE003	0.372(1)	−0.196(1)	51.610(4)	0.349(3)

[a] δ (mm/s) = isomer shift relative to metallic iron.
[b] ΔE_Q (mm/s) = quadrupole splitting.
[c] B_{hf} (T) = hyperfine field.
[d] Γ (mm/s) = line width.

FORC distributions below the Bc axis move toward the origin. This peak becomes narrower with increasing temperature but otherwise maintains the shape it had at room temperature (Figures 5a, 5b, and 5c). This progression is consistent with a decrease in the coercivity of hematite as a function of increasing temperature as has been observed by *Muxworthy and Dunlop* [2002] and *Carvallo and Muxworthy* [2006] and is due to internal crystal-line transformation [*Kletetschka et al.*, 2000b; *Dunlop and Kletetschka*, 2001; *Özdemir et al.*, 2002]. The small peak near the Bc and Bb origin that developed at 550°C in the FORC distribution is probably due to the transformation (reduction) of hematite to magnetite [*Dunlop and Özdemir*, 1997; *Carvallo et al.*, 2006] or the formation of maghemite [*De Boer and Dekkers*, 2001]. Maghemite (γ-Fe$_2$O$_3$) has high magnetic moment, spinel crystal structure and magnetic characteristics similar to magnetite (Fe$_3$O$_4$). The smooth distribution on the Bc axis from the origin up to 300 mT with a peak at 100 mT is visible at 650°C (Figure 5f) for all samples and, probably, represents the hematite that assumes low-coercivity characteristics at this temperature. This peak vanishes at 700°C in all samples, since all magnetic minerals lose their ferromagnetic/antiferromagnetic properties at such high temperatures (Figure 5g). Porous and Massive types show the same magnetic features with increasing temperature.

[23] Importantly, the hysteresis curves after annealing in helium atmosphere at 700°C are strongly different from the initial ones for all samples, meaning that this temperature produced structural changes in the samples. All FORCs measured at room temperature after the heating experiments in He show two peaks (Figures 5h, 5i, and 5j): (1) the "banana" shape peak or the linear crest below the Bc axis, respectively for Massive and Porous samples (this peak can be associated with hematite) and (2) a peak at the Bc and Bb origin. This peak probably represents a low-coercivity mineral (maghemite or magnetite) produced during the reduction of hematite during heating in absence of oxygen.

[24] Heating experiments in argon in the Kappa-bridge show an increase in susceptibility, consistent with generation of magnetite or maghemite. Thus reduction or phase changes occur using both instruments in reducing environments. However, the hysteresis parameters and FORCs from the sister samples annealed at 700°C in air (20%O$_2$) do not show the same changes, Furthermore, subsequent heating in a reducing (Ar) atmosphere did not form the low-coercivity component that was produced in reducing atmosphere with no prior annealing. Thus, heating to 700°C in air apparently produced an irreversible change that prevented formation of the low coercivity component.

[25] In summary, these hematite "bombs" of the Araguainha impact structure, if first heated in reducing atmosphere conditions, show the formation of a low-coercivity mineral. But if first heated in oxidizing atmosphere, they do not show the formation of the low-coercivity mineral, nor do they if reheated in a reducing (argon) atmosphere. This means that the virgin material was either not heated up to 700°C or was at an elevated temperature for too short a time for annealing. Otherwise, the samples would not present the low-coercivity peak in reducing atmosphere experiments.

[26] Mössbauer spectra at annealing conditions (Figures 3a and 3b, sample AE014) demonstrate the same pre-heating sextet, which shows pure hematite [*Gaviría et al.*, 2007]. Furthermore, the 2-theta peaks at ~36, ~54, ~57 and ~72 degrees (Figures 3a and 3b, sample AE014) of the XRD spectrum after heating are consistent with counting of pure hematite [*Gaviría et al.*, 2007]. In this sample, traces of maghemite can be inferred thanks to the presence of a spikes corresponding to the planes (111), (222) and (333) [*De Boer and Dekkers*, 2001].

[27] However, FORC results demonstrate that the samples are composed of pure hematite with traces below 1% of a low-coercivity component (magnetite/maghemite). The progression from SD-like to MD-like grain-size for these hematite samples is non-reversible and persists also after annealing. Thermo-magnetic treatments reveal that only a small part of hematite is altered to new magnetite/maghemite, and only on initial heating in a reducing atmosphere. Despite the low concentration of magnetite/maghemite produced by the heating experiments, it is clear that this trace amount contributes significantly to the FORC signal (Figures 5h and 5i). This is because maghemite and magnetite have a far stronger magnetic moment than does hematite.

4.3. Significance for This Material's Origin

[28] According to *Hippertt and Lana* [1998], Araguainha hematite "bombs" were formed by the melting and ejection of the Fe-rich sedimentary target rocks. Melting and ejection occur during the first and second stages of the impact cratering process, which is governed by the thermodynamics of shock compression and release [e.g., *Melosh*, 1989; *Pierazzo et al.*, 1997]. The first stage (contact/compression) begins when the projectile (e.g., meteorite) contacts the target-rocks, generating shock waves that propagate both in the projectile and the target-rocks [e.g., *Melosh*, 1989]. High pressures and temperatures (on order of tens GPa and few thousands of °C, respectively) produced by the shock-wave propagation promotes the vaporization of the projectile and part of the target rocks [e.g., *Melosh*, 1989]. In the next stage (excavation), the initial shock-wave energy is converted to kinetic energy, and complex interactions of the shock wave, the target rocks, and the subsequent rarefaction wave produce the excavation flow that opens the transient crater [*French*, 1998]. The voluminous amount of material driven out of the transient crater forms the proximal and distal ejecta deposits [e.g., *Melosh*, 1989]. This material is ejected as a mixture of vapor, molten materials and solid particles (rock fragments), which contrast in physical state, temperature and deformation. Considering these contrasts and the limitations of laboratorial experiments (e.g., rarely is possible to obtain vapor phase in laboratory impact experiments), both thermodynamic and thermochemical conditions of the ejecta flow remain debated in literature [e.g., *Melosh*, 1989; *French*, 1998].

[29] After deposition of ejected material, in the last stage of impact crater process (modification), a significantly part of the proximal ejecta deposit is driven toward the crater center forming the fallback deposits [e.g., *French*, 1998]. At Araguainha the fallback deposit is characterized by the polymict breccia observed in the central uplift [e.g., *von Engelhardt et al.*, 1992]. This breccia is composed of clasts with sizes ranging from centimeters to meters embedded in a fine-grained matrix. Most clasts are angular and composed of sedimentary rock, and less abundant are clasts of porphyritic granite, metamorphic basement, and iron oxide nodules. The polymict breccia deposit is located just above of the impact melt sheet [e.g., *von Engelhardt et al.*, 1992; *Machado et al.*, 2009]. The impact melt sheet is exclusively formed by granitic molten rocks, and geochemical data suggests that crystallization temperature of this melt was around of 1100°C [*von Engelhardt et al.*, 1992].

[30] Could the hematite nodules have originated as *Hippertt and Lana* [1998] proposed? Impact temperature would have been high enough to melt hematite (melting temperature is ~1500°C) so ejection of molten hematite and inclusion as nodules in the polymict breccia after return from proximal deposits seems plausible. However, unknown is a related mechanism for producing pure hematite, whether the nodules, especially the porous ones, could have preserved their delicate features during the probably violent breccia deposition, and whether they could have been quenched and remained cool during the process.

[31] Our results for hematite nodules found in the Araguainha polymict breccia show significant differences in magnetic properties before and after heating. This suggests that those nodules were never heated above 700°C in either oxygen rich or oxygen poor environments. If they had experienced elevated temperatures in a reducing environment, the low coercivity high susceptibility phase should have been detected in our initial room temperature experiments; if heating had been sufficiently long in an oxidizing environment, our reducing atmosphere experiments would not have generated that phase. The onset of magnetite/maghemite generation at 400°C suggests a lower bound for the maximum temperature reached by these samples. On the other hand, temperatures below 400°C are easily reached in hydrothermal systems present in impact craters [*Pirajno*, 2010, and references therein]. At Araguainha, crystallization of the melt sheet could have release enough heat to start and maintain circulation of hydrothermal fluids. For example, *von Engelhardt et al.* [1992] suggested that some features observed in the polymict breccia, such as silification and deposition of hematite, could be related to low temperature fluid circulation (on order of the diagenetic temperatures). In fact, the Araguainha's hematites are similar to the botryoidal hematites found in some iron-manganese deposits, which were formed by hydrothermal vein systems [*Wernicke and Lippolt*, 1993, and references therein]. Moreover, estimates for fluid temperatures in those iron-manganese deposits suggest that the botryoidal hematite formed below 150°C [*Wernicke and Lippolt*, 1993], similar to that of for diagenetic process.

[32] If the hematites from Araguainha have a hydrothermal origin, the Martian hematite nodules could be associated with impact craters. This explanation

should be explored further via geochemical analysis of these rocks and their environment to determine redox and hydrothermal conditions after the impact.

5. Conclusions

[33] Impact ejected bombs with aerodynamic features are observed at many meteoritic impact structures. However, such material, which is dispersed inside and outside the crater, varies from millimeters to few centimeters in size, and is essentially composed of glass formed by melting and mixing of target-rocks and rarely from the bolide body itself. By contrast, the material sampled for this study varies in size from 5 to 50 cm in diameter, is located only in the center of the Araguainha crater (polymict breccias deposit) and has the peculiar hematitic composition. Furthermore, the original iron-rich source is problematic, the most likely being the red sandstones now situated in the collar of the structure, but one would expect some amount of quartz or glass in the analyzed material, which we did not observe. The impactor cannot be the source either. For such a size of impact, the meteorite evaporates and disperses in the atmosphere as powder after the collision with the surface of the Earth, rendering impossible the preservation of the original material.

[34] The results of our thermomagnetic experiments are consistent with another process that produced these hematite "bombs" after the Araguainha bolide body impact. We speculate here that they were generated by post-impact hydrothermal circulation, most likely driven by residual heat from the impact. If this is the case, the material was likely not heated above 400°C. Indeed the Araguainha's hematites are similar to the botryoidal hematites found on some iron-manganese deposits, which were formed by several hydrothermal veins systems at low temperatures. Even if the weathering conditions do not permit a clear identification of the hydrothermal veins within the Araguainha's polymict breccias, the hydrothermal flow in this kind of impact structure is usually along fracture systems. The hydrothermal origin of the Araguainha's hematites has important implications to understanding the processes that follow an impact of such dimensions and, by extension to other planets with water (Mars in particular), processes that may have operated there.

Acknowledgments

References

Acton, G., A. Roth, and K. L. Verosub (2007), Analyzing micromagnetic properties with FORCIT software, *Eos Trans. AGU*, *88*(21), 230, doi:10.1029/2007EO210004.

Acuña, M. H., et al. (1999), Global distribution of crustal magnetization discovered by the Mars Global Surveyor MAG/ER experiment, *Science*, *284*(5415), 790–793, doi:10.1126/science.284.5415.790.

Arkani-Hamed, J. (2002), Magnetization of the Martian crust, *J. Geophys. Res.*, *107*(E5), 5032, doi:10.1029/2001JE001496.

Arvidson, R. E., et al. (2006), Nature and origin of the hematite-bearing plains of Terra Meridiani based on analyses of orbital and Mars Exploration rover data sets, *J. Geophys. Res.*, *111*, E12S08, doi:10.1029/2006JE002728.

Carporzen, L., S. A. Gilder, and R. J. Hart (2005), Paleomagnetism of Vredefort meteorite crater and implications for craters on Mars, *Nature*, *435*(7039), 198–201, doi:10.1038/nature03560.

Carvallo, C., and A. R. Muxworthy (2006), Low-temperature first-order reversal curve (FORC) diagrams for synthetic and natural samples, *Geochem. Geophys. Geosyst.*, *7*, Q09003, doi:10.1029/2006GC001299.

Carvallo, C., A. R. Muxworthy, and D. J. Dunlop (2006), First-order reversal curve (FORC) diagrams of magnetic mixtures: Micromagnetic models and measurements, *Phys. Earth Planet. Inter.*, *154*, 308–322, doi:10.1016/j.pepi.2005.06.017.

Catling, D. C., and J. M. Moore (2003), The nature of coarse-grained crystalline hematite and its implications for the early environment of Mars, *Icarus*, *165*, 277–300, doi:10.1016/S0019-1035(03)00173-8.

Day, R., M. D. Fuller, and V. A. Schmidt (1977), Hysteresis properties of titanomagnetites: Grain size and composition dependence, *Phys. Earth Planet. Inter.*, *13*, 260–267, doi:10.1016/0031-9201(77)90108-X.

De Boer, C. B., and M. J. Dekkers (2001), Unusual thermomagnetic behaviour of haematites: Neoformation of a highly magnetic spinel phase on heating in air, *Geophys. J. Int.*, *144*, 481–494, doi:10.1046/j.0956-540X.2000.01333.x.

Dunlop, D. J. (2002), Theory and application of the Day plot (M_{rs}/M_s versus H_{cr}/H_c) 1. Theoretical curves and tests using titanomagnetite data, *J. Geophys. Res.*, *107*(B3), 2056, doi:10.1029/2001JB000486.

Dunlop, D. J., and J. Arkani-Hamed (2005), Magnetic minerals in the Martian crust, *J. Geophys. Res.*, *110*, E12S04, doi:10.1029/2005JE002404.

Dunlop, D. J., and G. Kletetschka (2001), Multidomain hematite: A source of planetary magnetic anomalies?, *Geophys. Res. Lett.*, *28*, 3345–3348, doi:10.1029/2001GL013125.

Dunlop, D. J., and Ö. Özdemir (1997), *Rock Magnetism: Fundamentals and Frontiers*, 573 pp., Cambridge Univ. Press, New York, doi:10.1017/CBO9780511612794.

French, B. M. (1998), *Traces of Catastrophe: A Handbook of Shock-metamorphic Effects in Terrestrial Meteorite Impact Structures*, 130 pp., Lunar Planet. Inst., Houston, Tex.

French, B. M. (2004), The importance of being cratered: The new role of meteorite impact as a normal geological process, *Meteorit. Planet. Sci.*, *39*, 169–197, doi:10.1111/j.1945-5100.2004.tb00335.x.

Gaviría, J. P., A. Bohé, A. Pasquevich, and D. M. Pasquevich (2007), Hematite to magnetite reduction monitored by Mössbauer spectroscopy and X-ray diffraction, *Phys. B*, *389*, 198–201, doi:10.1016/j.physb.2006.07.056.

Hammerschmidt, K., and W. von Engelhardt (1995), Ar/Ar dating of the Araguainha impact structure, Mato Grosso, Brazil, *Meteoritics*, *30*, 227–233.

Harrison, R. J., and J. M. Feinberg (2008), FORCinel: An improved algorithm for calculating first-order reversal curve distributions using locally weighted regression smoothing, *Geochem. Geophys. Geosyst.*, *9*, Q05016, doi:10.1029/2008GC001987.

Hippertt, J., and C. Lana (1998), Aerial crystallization of hematite in impact bombs from the Araguainha astrobleme, Mato Grosso, central Brazil, *Meteorit. Planet. Sci.*, *33*, 1303–1309, doi:10.1111/j.1945-5100.1998.tb01314.x.

Kletetschka, G., P. J. Wasilewski, and P. T. Taylor (2000a), Hematite vs. magnetite as the signature for planetary magnetic anomalies?, *Phys. Earth Planet. Inter.*, *119*, 259–267, doi:10.1016/S0031-9201(00)00141-2.

Kletetschka, G., P. J. Wasilewski, and P. T. Taylor (2000b), Unique thermoremanent magnetization of multidomain sized hematite: Implications for magnetic anomalies, *Earth Planet. Sci. Lett.*, *176*, 469–479, doi:10.1016/S0012-821X(00)00016-9.

Koeberl, C. (2006), Impact processes on the early Earth, *Elements*, *2*, 211–216, doi:10.2113/gselements.2.4.211.

Lana, C. C., C. R. Souza Filho, Y. R. Marangoni, E. Yokoyama, R. I. F. Trindade, E. Thover, and W. U. Reimold (2007), Insights into the morphology, geometry, and post-impact erosion of the Araguainha peak-ring structure, central Brazil, *Geol. Soc. Am. Bull.*, *119*(9–10), 1135–1150, doi:10.1130/B26142.1.

Lana, C. C., C. R. Souza Filho, Y. R. Marangoni, E. Yokoyama, R. I. F. Trindade, E. Thover, and W. U. Reimold (2008), Structural evolution of the 40 km wide Araguainha impact structure, central Brazil, *Meteorit. Planet. Sci.*, *43*, 701–716, doi:10.1111/j.1945-5100.2008.tb00679.x.

Larrasoaña, J. C., C. Gonzalvo, E. Molina, S. Monechi, S. Ortiz, F. Tori, and J. Tosquella (2007), Diagenetic formation of greigite and pyrrhotite in gas hydrate marine sedimentary systems, *Earth Planet. Sci. Lett.*, *261*, 350–366, doi:10.1016/j.epsl.2007.06.032.

Leonhardt, R. (2006), Analyzing rock magnetic measurements: The RockyMagAnalyser 1.0 software, *Comput. Geosci.*, *32*, 1420–1431, doi:10.1016/j.cageo.2006.01.006.

Machado, R., C. Lana, G. Stevens, C. R. Souza-Filho, and W. U. Reimold (2009), Generation, mobilization and crystallization of impact-induced alkali-rich melts in granitic target rocks: Evidence from the Araguainha impact structure, central Brazil, *Geochim. Cosmochim. Acta*, *73*(23), 7183–7201, doi:10.1016/j.gca.2009.08.029.

Melosh, H. J. (1989), *Impact Cratering: A Geologic Process*, 245 pp., Oxford Univ. Press, New York.

Mohit, P. S., and J. Arkani-Hamed (2004), Impact demagnetization of Martian crust, *Icarus*, *168*(2), 305–317, doi:10.1016/j.icarus.2003.12.005.

Muxworthy, A. R., and D. J. Dunlop (2002), First-order reversal curve (FORC) diagrams for pseudo-single-domain magnetites at high temperature, *Earth Planet. Sci. Lett.*, *203*, 369–382, doi:10.1016/S0012-821X(02)00880-4.

Muxworthy, A. R., and A. P. Roberts (2006), First-order reversal curve (FORC) diagrams, in *Encyclopedia of Geomagnetism and Paleomagnetism*, edited by D. Gubbins and E. Herrero-Bervera, pp. 266–272, Springer, New York.

Muxworthy, A. R., J. G. King, and D. Heslop (2005), Assessing the ability of first-order reversal curve (FORC) diagrams to unravel complex magnetic signals, *J. Geophys. Res.*, *110*, B01105, doi:10.1029/2004JB003195.

Özdemir, Ö., D. J. Dunlop, and B. M. Moskowitz (2002), Changes in remanence, coercivity and domain state at low temperature in magnetite, *Earth Planet. Sci. Lett.*, *194*, 343–358, doi:10.1016/S0012-821X(01)00562-3.

Petrovský, E., V. Kropàček, M. J. Dekkers, C. der Boer, V. Hoffman, and A. Ambatiello (1996), Transformation of hematite to maghemite as observed by changes in magnetic parameters: Effects of mechanical activation, *Geophys. Res. Lett.*, *23*, 1477–1480, doi:10.1029/96GL01411.

Pierazzo, E., A. M. Vickery, and H. J. Melosh (1997), A reevaluation of impact melt production, *Icarus*, *127*(2), 408–423, doi:10.1006/icar.1997.5713.

Pike, C. R., A. P. Roberts, and K. L. Verosub (1999), Characterizing interactions in fine magnetic particle systems using first order reversal curves, *J. Appl. Phys.*, *85*(9), 6660–6667, doi:10.1063/1.370176.

Pirajno, F. (2010), *Hydrothermal Processes and Mineral Systems*, 1250 pp., Springer, New York.

Roberts, A. P., C. R. Pike, and K. L. Verosub (2000), First-order reversal curve diagrams: A new tool for characterizing the magnetic properties of natural samples, *J. Geophys. Res.*, *105*, 28,461–28,475, doi:10.1029/2000JB900326.

Roberts, A. P., F. Florindo, J. C. Larrasoaña, M. A. O'Regan, and X. Zhao (2010), Complex polarity pattern at the former Plio–Pleistocene global stratotype section at Vrica (Italy): Remagnetization by magnetic iron sulphides, *Earth Planet., Sci. Lett.*, *292*, 98–111, doi:10.1016/j.epsl.2010.01.025.

Rochette, P., J. P. Lorand, G. Fillion, and V. Sautter (2001), Remanent magnetization of basaltic Shergottites carried by pyrrhotite: A changing perspective on Martian magnetism, *Earth Planet. Sci. Lett.*, *190*, 1–12, doi:10.1016/S0012-821X(01)00373-9.

Rochette, P., G. Fillion, R. Ballou, F. Brunet, B. Ouldiaf, and L. Hood (2003), High pressure magnetic transition in pyrrhotite and impact demagnetization on Mars, *Geophys. Res. Lett.*, *30*(13), 1683, doi:10.1029/2003GL017359.

Shoemaker, E. M. (1977), Why study impact craters?, in *Impact and Explosion Cratering*, edited by D. J. Roddy et al., pp. 1–10, Pergamon, New York.

von Engelhardt, W., S. K. Matthäi, and J. Walzebuck (1992), Araguainha impact crater, Brazil, I. The interior part of the uplift, *Meteoritics*, *27*, 442–457.

Weaver, R., A. P. Roberts, and A. J. Barker (2002), A late diagenetic (syn-folding) magnetization carried by pyrrhotite: Implications for paleomagnetic studies from magnetic iron sulphide-bearing sediments, *Earth Planet. Sci. Lett.*, *200*, 371–386, doi:10.1016/S0012-821X(02)00652-0.

Wernicke, R. S., and H. J. Lippolt (1993), Botryoidal hematite from the Schwarzwald (Germany) heteregeneous uranium distributions and their bearing on the helium dating method, *Earth Planet. Sci. Lett.*, *114*, 287–300, doi:10.1016/0012-821X(93)90031-4.

Wernicke, R. S., and H. J. Lippolt (1997), (U + Th)-He evidence of Jurassic continuous hydrothermal activity in the Schwarzwald basement, Germany, *Chem. Geol.*, *138*, 273–285, doi:10.1016/S0009-2541(97)00020-X.